Comparison of Interior and Surface PM Machines Equipped With Fractional-Slot Concentrated Windings for Hybrid Traction Applications

Patel B. Reddy, *Member, IEEE*, Ayman M. El-Refaie, *Senior Member, IEEE*, Kum-Kang Huh, *Member, IEEE*, Jagadeesh K. Tangudu, *Member, IEEE*, and Thomas M. Jahns, *Fellow, IEEE*

***Abstract*—Electric drive systems, which include electric machines and power electronics, are a key enabling technology for advanced vehicle propulsion systems that reduce the petroleum dependence of the ground transportation sector. To have significant effect, electric drive technologies must be economical in terms of cost, weight, and size while meeting performance and reliability expectations. This paper will provide details of the design, analysis, and testing of two permanent magnet (PM) machines that were developed to meet the FreedomCar 2020 specifications. The first machine is an interior PM (IPM) machine and the second machine is a surface PM (SPM) machine. Both machines are equipped with fractional-slot concentrated windings (FSCW). The goal of this paper is to provide a quantitative assessment of how achievable this set of specifications is, as well as a comparison with the state of the art. This paper will also quantitatively highlight the tradeoffs between IPM and SPM FSCW machines especially in the context of traction applications.**

***Index Terms*—Comparison, concentrated, fractional-slot, high speed, interior, machines, permanent magnet (PM), surface, traction, windings.**

I. Introduction

ELECTRIC drive systems, which include electric machines and power electronics, are a key enabling technology for advanced vehicle propulsion systems that reduce the petroleum dependence of the ground transportation sector. To have significant effect, electric drive technologies must be economical in terms of cost, weight, and size while meeting performance and reliability expectations.

The objective of this paper is to develop high power density, high-efficiency permanent magnet (PM) motors at a lower cost. The FreedomCar 2020 required motor set of specifications is summarized in Table I and Fig. 1. It can be seen that this is a very challenging set of specifications including maximum speed of 14 000 r/min, continuous power of 30 kW over 20–100% speed range, peak power of 55 kW for 18 s at 20% speed, minimum efficiency of 95% over 10–100% speed range, 105 °C cooling inlet temperature, fixed nominal 325-V dc source, approximately twice the power densities (at maximum speed) of the present state of the art (SoA) [1], and an aggressive cost target of US$275 per unit for mass manufacturing in quantities of 100 000 s.

This paper presents and compares two PM designs equipped with fractional-slot concentrated windings. The first is a fractional-slot concentrated winding (FSCW) interior PM (IPM) machine, while the second is an FSCW surface PM (SPM) machine. These high-performance FSCW PM machines have been developed, built, and tested to address the challenging performance metrics imposed by the FreedomCar 2020 advanced traction motor specifications. Significant efforts have been focused on trying to meet the demanding efficiency specifications and

TABLE I
FreedomCAR 2020 Advanced Motor Performance Requirements

Requirement	Target	Condition
Minimum top speed	14,000 rpm	
Peak output power	55 kW for 18sec	at 20% speed and nominal voltage
Continuous output power	30 kW	at 20~100% speed and nominal voltage
Weight	≤ 35 kg	
Volume	≤ 9.7 L	
Unit cost	≤ $275	in quantities of 100,000
Operating DC bus voltage	200~450V, 325V nominal	
Maximum phase current	400Arms	
Characteristic current	< Max. current	
Efficiency	> 95%	at 10~100% speed for 20% rated torque
Line-to-line Back-EMF	< 600V peak	at 100% speed
Torque pulsation	< 5% peak torque	at any speed
Ambient operating temp.	-40~140°C	outside housing
Coolant inlet temperature	105°C	
Max. coolant flow rate	10 liters/min	
Max. coolant pressure drop	2 psi	
Max. coolant inlet pressure	20 psi	
Min. isolation impedance	1MΩ	terminals to ground

Manuscript received August 1, 2011; revised January 7, 2012; accepted March 19, 2012. Date of publication May 3, 2012; date of current version July 27, 2012. This work was supported by the Department of Energy under Award DE-FC26-07NT43122. Paper no. TEC-00338-2011.

P. B. Reddy, A. M. El-Refaie, and K.-K. Huh are with the Electrical Machines Laboratory, General Electric Global Research Center, Niskayuna, NY 12309 USA (e-mail: reddy@ge.com; elrefaie@research.ge.com; huhk@ge.com).

J. K. Tangudu was with the Department of Electrical and Computer Engineering, University of Wisconsin-Madison, Madison, WI 53706 USA. He is now with the United Technologies research Center, East Hartford, CT 06118 USA (e-mail: jagadeesh.tangudu@gmail.com).

T. M. Jahns is with the Department of Electrical and Computer Engineering, University of Wisconsin-Madison, Madison, WI 53706 USA (e-mail: jahns@engr.wisc.edu).

Color versions of one or more of the figures in this paper are available online at http://ieeexplore.ieee.org.

Digital Object Identifier 10.1109/TEC.2012.2195316

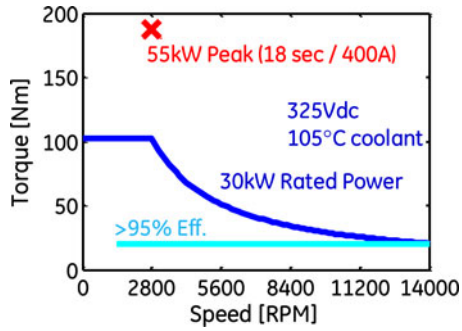

Fig. 1. FreedomCar 2020 motor specified torque–speed curve.

Fig. 2. Stator of the FSCW-IPM machine.

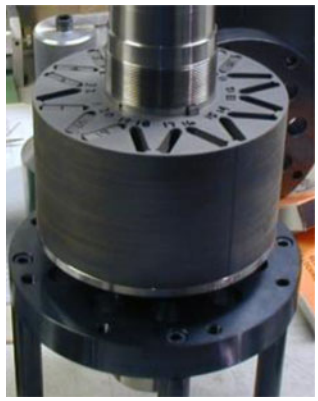

Fig. 3. Rotor of the FSCW-IPM machine.

minimizing the losses. Losses in the copper, iron, and magnets are investigated under a variety of operating conditions, with a focus on high-speed operation. Finite-element analysis (FEA) is utilized to predict the loss components in these machines during the design stage.

Experimental results for both machines will be presented. These results will be compared to their respective predictions from the FEA models. The testing of the two machines has been done at two different locations (using two different lab setups) under different thermal conditions. Due to the difference in mechanical losses between the two lab setups, and in order to have a fair comparison, the focus is mainly on comparing the electrical performance in terms of output power and losses. Key conclusions are drawn based on power density, electrical efficiencies, losses, and torque.

II. IPM Machine

Segmented stator structures equipped with FSCW have numerous well-established advantages associated with this type of windings including high slot fill factor, short-end turns, and high efficiency and power density [2]–[9]. A ten-pole, 12-slot IPM machine using high-strength sintered NdFeB magnets is built with 12 individually wound tooth structures, making it a double-layer winding pattern. The stator structure along with a couple of teeth of the IPM machine is shown in Fig. 2. The rotor is made from laminations with the magnets forming a V-shape within the rotor as shown in Fig. 3. The stator and the rotor laminations belong to the HF10 material, which is known to have considerably a lower thickness value of 0.25 mm. This lower thickness value contributes to the reduced iron loss coefficients in the laminations, helping to reduce the iron losses at top speeds, where in the frequencies exceed values of 1 kHz.

Every teeth segment of the stator laminations is punched and stacked to provide the building block of the machine. The copper winding is wound around each individual teeth segment to create the double-layer configuration. The final assembled stator is shown in Fig. 2. The process of segmentation is able to reach slot fill factor values of 50% (defined as ratio of the copper area to the total slot area).

The assembly of the stator structure begins with a single teeth structure, with the winding already wound around it. The adjacent teeth structures are added in either ends, where in grooves are present in the stator yoke to form a well-defined pattern. The structure with two assembled teeth segments with windings is shown in Fig. 2. Repeating this structure over the entire 360° forms the complete stator, which is also shown in Fig. 2.

The magnets are made out of Vacodym 890 material and have a magnetic remanence of 1.07 T at room temperature, a relative permeability of 1.037 and a maximum operating temperature of 240 °C.

The rotor geometry has gone through a multivariable optimization in order to achieve the best torque density in the machine along with the best efficiency. The parameters chosen were the rotor magnet locations, thickness along with pole arcs of the magnets. The bridge and center-post thicknesses have been optimized for mechanical integrity at 150% times of the maximum speed of the rotor. The rotor structure is made with two nonmagnetic end-plates to hold the rotor laminations together. The effect of the end-plates on the motor performance has been described in [10].

The operating points in terms of the *d*- and *q*-axis currents of the FSCW-IPM machine along with the predicted loss components under rated-load conditions (30 kW) are shown in Figs. 4 and 5. Combination of 2-D FEA and 3-D FEA was used to evaluate losses in the magnets and in the stator and rotor laminations (including both hysteresis and eddy current losses). The magnet losses are the loss components arising out of the 3-D finite-element runs with the stator current excitation and magnet segmentation, while it is seen that 2-D FEA is quite adequate for

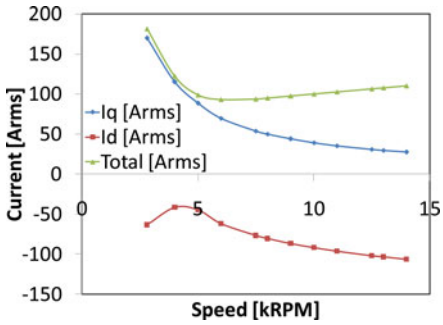

Fig. 4. Predicted I_d–I_q current over the speed range above 2800 r/min under rated-load conditions (30 kW) for FSCW-IPM machine.

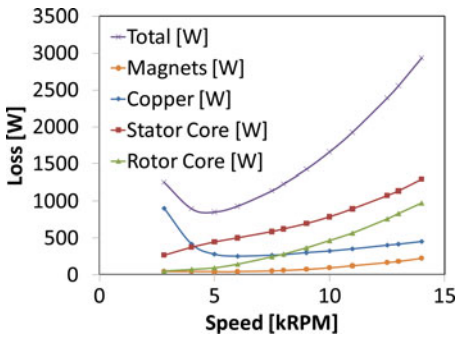

Fig. 5. Predicted losses over the speed range under rated-load condition (30 kW) for FSCW-IPM machine.

the iron loss calculations. From Fig. 4, it can be seen that as expected, the q-axis current decreases with speed (due to the lower torque required to maintain constant power operation), [4], [5], while the d-axis current increases with speed due to flux weakening to keep the voltage within the available limits (based on 325-V nominal dc-bus voltage).

The predicted losses in the IPM machine under rated-load operating conditions (30 kW) are shown in Fig. 5. It can be seen that due to axial segmentation of the magnets as well as the fact the magnets are buried in the rotor laminations relatively far away from the air gap, the magnet losses are fairly low across the whole speed range [8]. Since much attention has been paid to reducing the ac losses in the windings (mainly in terms of the strand size and Litz wire construction), the copper losses are mainly dependent on the current and, as can be seen, the copper loss variation is very similar to the total current variation shown in Fig. 4. Also the use of FSCW helps in reducing the copper losses due to the reduction in the copper losses in the end windings.

It can also be seen in Fig. 5 that the stator and rotor core losses are the dominant components and form the major portion of the total losses in the machine. Both increase with speed as expected. The rich space harmonic contents in the FSCW contribute to higher core losses in both the rotor and stator [9]–[12]. Also, the presence of the rotor "slots" (where the magnets reside) introduces additional harmonics, which cause higher stator core losses. In addition, the higher pole count in the FSCW machines (ten poles in this case) contributes to the result that the total losses at higher speeds (especially at 14000 r/min) are

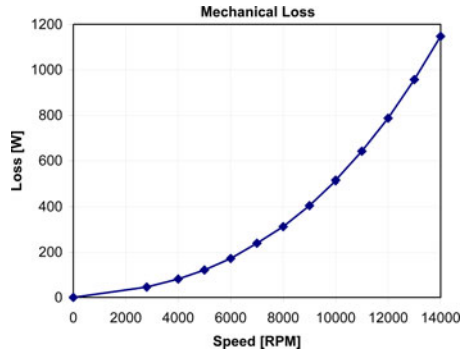

Fig. 6. Experimental measured mechanical losses with unmagnetized magnets.

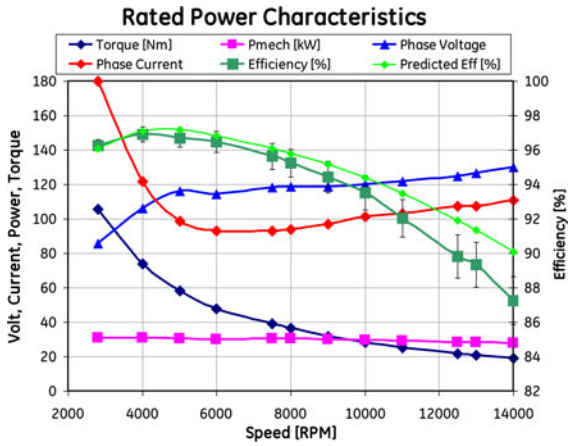

Fig. 7. Experimental results from the FSCW-IPM machine under rated-load condition.

significant. The total predicted efficiency shown later in this paper is well above the minimum requirement over most of the speed range, but at the top speeds, the predicted efficiency drops below the required minimum of 95%.

III. Experimental Results of IPM Machine

In order to separate mechanical and electrical losses, the machine was first built using unmagnetized magnets. Fig. 6 shows the test results for the machine with unmagnetized magnets. Based on the test results, more modifications are planned to reduce mechanical losses at 14 000 r/min by ∼35%. These include using lower loss bearings, lower loss seals, and reducing churning losses due to the rotor inner bore cooling.

Next, the machine with magnetized magnets was tested. Fig. 7 shows several measured machine performance parameters at rated power as well as a comparison of measured and predicted efficiency. It can be seen that the voltage limit is reached at approximately 5000 r/min, which represents the machine corner speed. The output mechanical power (Pmech) is kept in the vicinity of 32 kW over the entire speed range, while the overall efficiency is higher than 95% over a speed range of 2800–8500 r/min. The results show that the machine meets both peak and steady-state power requirements.

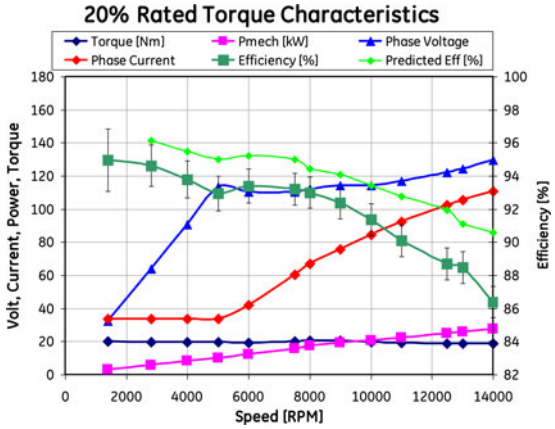

Fig. 8. Experimental results from the FSCW-IPM machine under partial-load conditions.

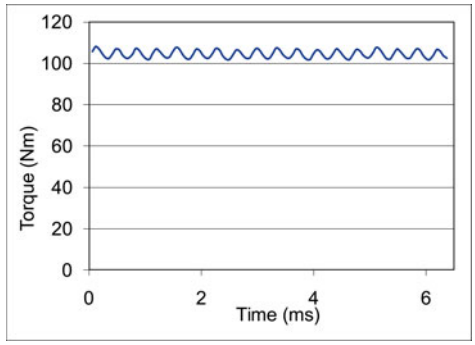

Fig. 9. Finite element predictions of the torque versus time at 2800 r/min, 33 kW in the FSCW-IPM machine.

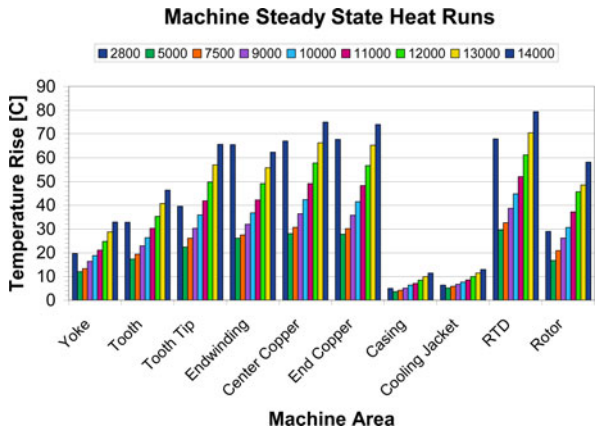

Fig. 10. Measured temperature rises in various locations in the FSCW-IPM machine.

Mechanical losses at higher speeds are seen to cause deviation from the predictions at higher speeds. At the top speed, the experimental efficiency is approximately 87%, which is approximately 3% lower than the predictions, with most of the drop attributed to the mechanical causes cited previously.

The experimental results under the partial-load 20% rated torque conditions over a speed range of 1400–14 000 r/min are shown in Fig. 8. A higher difference is seen in the predicted and experimental efficiencies under the partial-load conditions. The machine is able to exceed the partial-load minimum efficiency requirement of 95% at the lower speeds, while it is able to deliver at least 93% efficiency up to a speed of 8000 r/min. The efficiency drops to ~87% at 14 000 r/min. One of the major suspects for causing the lower efficiency is the presence of the mechanical losses in the system along with the current regulation. Since the FSCW-IPM machine has more harmonics in the back electromotive force (EMF) waveform, pure sinusoidal current regulation might not be enough to achieve the required partial-load efficiencies. In these machines, the presence of harmonics allows for improvements in efficiencies with the introduction of current profiling. In [13] and [14], the authors have demonstrated the potential of optimal current profiling to improve the efficiency and the torque production in electric machines.

The torque ripple is expected to be very low in the FSCW-IPM machines [2] due to the fact that the lowest common multiple of the stator slots and the rotor poles being very high. This rule [2] is justified by the torque waveform in the machine at a speed of 2800 r/min, while providing a power of 33 kW. The peak–peak torque ripple is seen to be 5.5%, while the average is 103.2 N·m. As shown in Fig. 9.

As part of the machine test sequence, steady-state heat runs were performed (times of runs were between 45 min and 1 h, time taken to reach steady-state temperatures in windings) on the FSCW-IPM machine from 2800 to 14 000 r/min under rated-load conditions. The steady-state temperature rise in the machine measured in different locations in the machine (yoke, teeth, teeth-tip, end winding, center of the windings, copper end region in the slot, the casing, the cooling jacket, and the rotor) is shown in Fig. 10. The machine was able to successfully withstand the temperature rise in the machine under all the operating conditions, with the top temperatures being within the insulation limits. The maximum temperature rises was seen in the copper regions, mainly the end-winding portion along with the slot regions inside the slots.

With a coolant temperature of 105 °C, the end-winding temperature would reach approximately 175–185 °C, well within the 220–240 °C temperature limits for the Class C insulation selected for the machine's magnet wire. Although the teeth tips also reach similar temperatures under some of the operating conditions, heat extraction through the laminations is easier since there is no insulation in the thermal path.

IV. SPM Machine

Based on the FSCW-SPM machine models developed in [4] and [15], closed-form analysis has been used in the machine design process. The final design of the FSCW-SPM machine is based on the FreedomCar advanced traction motor specifications that are summarized in Table I. The design and fabrication of the FSCW-SPM machine has been discussed in [16] and will not be repeated here. Instead, the high-level details are presented.

The constraint on the maximum back-EMF voltage of 600 V(pk) line-to-line at the top speed of 14 000 r/min is difficult to meet in the absence of magnetic saliency. In [17], the special challenges associated with designing an SPM machine to meet

Fig. 11. Stator of FSCW-SPM machine.

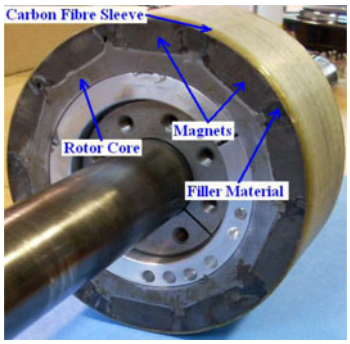

Fig. 12. Rotor of FSCW-SPM machine.

the FreedomCar power density requirements while simultaneously satisfying the maximum current and maximum back-EMF constraints have been investigated. As a result, the maximum back-EMF constraint was relaxed to 800 V (pk) line-to-line for this machine design exercise.

Similar to the FSCW-IPM machine, the FSCW-SPM machine has 10 poles and 12 slots. The stator structure is segmented as shown in Fig. 11. The stator laminations are made from HF10 material, which has also been used in the IPM motor. The stator of the SPM shares the manufacturing and assembly process as the stator of the IPM motor. On the other hand, the rotor assembly uses a laminated rotor core with ten flat surfaces to mount the segmented bread-loaf magnets. The magnets are high-strength sintered NdFeB magnets, belonging to the same Vacodym890 material used in the IPM motor. The magnets are segmented both circumferentially and axially in order to minimize the eddy current losses. Carbon fiber banding is tightly wound around the rotor outer periphery to provide the required structural containment at high rotor speeds. A view of the final rotor assembly is provided in Fig. 12. A view of the complete cross section is shown in Fig. 13.

The variation of the operating currents in the *d*- and *q*-axis in the FSCW-SPM machine under rated power conditions, similar to the IPM case, is shown in Fig. 14. It can be seen that, compared to the FSCW-IPM machine, flux weakening begins at lower speeds due to the higher magnet flux linkage.

The predicted losses of the FSCW-SPM machine under rated-load conditions (30 kW) are shown in Fig. 15. The SPM machine has a different loss picture compared to the IPM configuration. The majority of the losses occur in the magnets and the stator

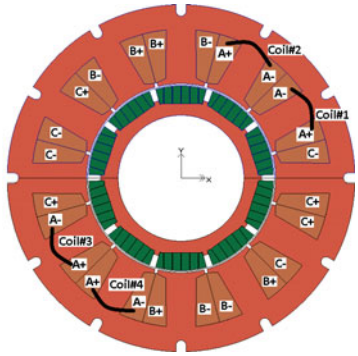

Fig. 13. Cross section of FWCW-SPM machine.

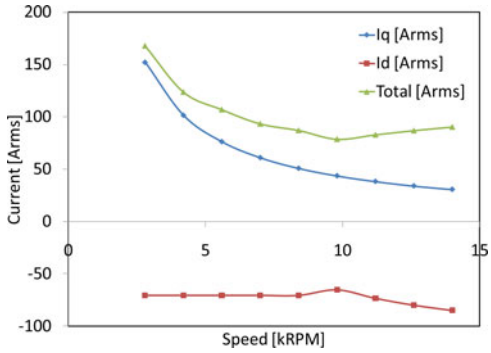

Fig. 14. Predicted I_d–I_q current over the speed range above 2800 r/min under rated-load conditions (30 kW) for FSCW-SPM machine.

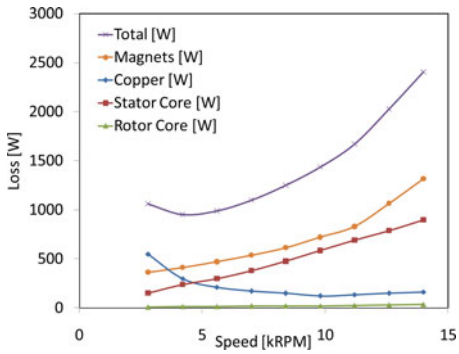

Fig. 15. Predicted losses over the speed range under rated-load condition (30 kW) for FSCW-SPM machine.

core, while the rotor core and copper losses are significantly lower. Despite the axial and circumferential segmentation, the magnets mounted in the air gap are exposed to all the harmonics arising from the concentrated windings. These magnet losses are unavoidable and are challenging to dissipate because of the lack of good convection paths aggravated by the presence of the carbon fiber retaining ring around the magnets.

The measured efficiency under partial-load conditions is shown later in Fig. 27. The experimental efficiency is in the range 93–95% for tested speeds up to 5000 r/min and closely matches the analytical and finite-element results.

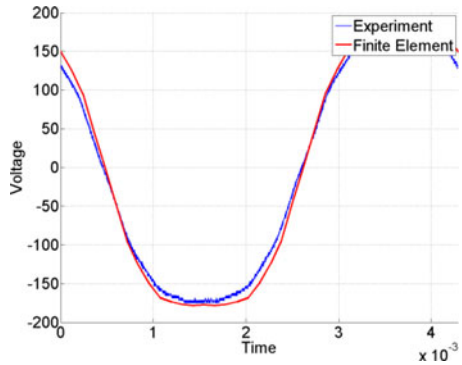

Fig. 16. Experimental back EMF for FSCW-SPM machine at 2800 r/min for 50 °C operation.

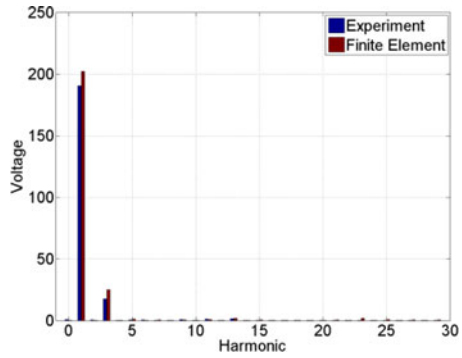

Fig. 17. Harmonic spectrum of back EMF for FSCW-SPM machine at 2800 r/min for 50 °C operation.

V. Experimental Results of SPM Machine

As previously mentioned, the SPM machine was tested using a different lab setup than the IPM machine. One of the issues with the testing was the constraints on the dynamometer machine. With the maximum speed of the dyno machine limited to 6000 r/min, all testing on the device-under-test machine has been limited to 5800 r/min. Additionally, the absence of liquid cooling for the stator placed additional thermal stress on the machine in terms of the operating temperatures. The only cooling available for the test machine was forced air cooling. However, the machine was tested at room temperature, which allowed for quite a bit of temperature margin in the machine.

The comparison of the open-circuit back-EMF waveform together with the harmonic spectrum is shown in Figs. 16 and 17, respectively. The experimental back EMF is approximately 6% lower than the predictions at 60 °C (magnet operating temperature). The harmonic spectrum also shows the clean nature of the phase back EMF of the SPM machine, allowing for better current regulation compared to the IPM machine. The distortion observed in the back-EMF waveform is known to arise from the space harmonic present in the rotor.

Fig. 18 shows the measured performance of the SPM machine under full load up to a speed of 5800 r/min. The machine is able to produce a power of 30 kW over this speed range while operating from a dc-bus voltage of 300 V_{dc}. Moreover, the finite element predicted power is seen to be higher than the experimentally measured power. One of the major reasons for this

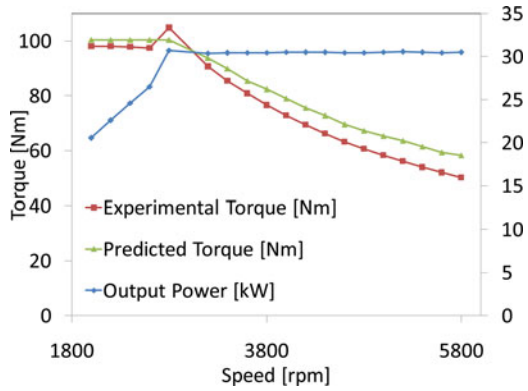

Fig. 18. Measured torque and power performance of the FSCW-SPM machine under rated-load conditions.

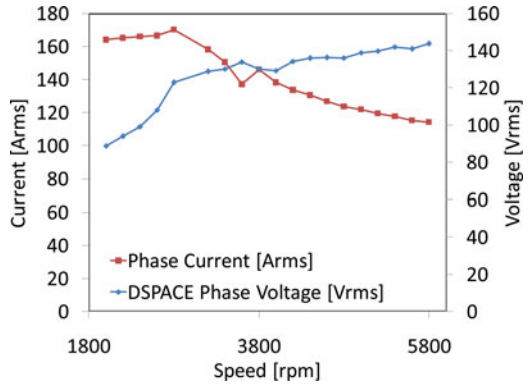

Fig. 19. Measured voltage and current of the FSCW-SPM machine under rated-load conditions.

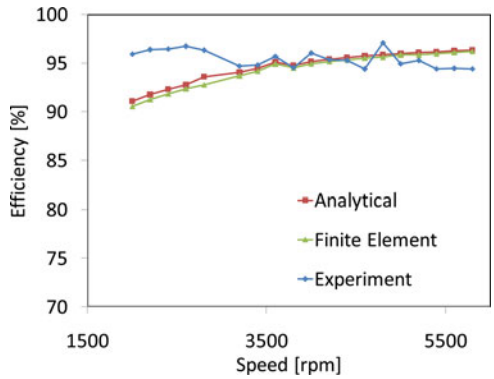

Fig. 20. Measured efficiency of the FSCW-SPM machine under rated-load condition.

discrepancy is the lower back EMF that was previously mentioned. The equivalent phase RMS voltage and the phase current are shown in Fig. 19. The current is limited to a maximum of 170 A_{rms}, while the voltage is limited to an equivalent dc-bus voltage of 300 V.

Fig. 20 shows a comparison of the analytical and finite-element predictions and the experimental efficiency values under rated power conditions, as described previously. The FSCW-SPM machine delivers measured efficiency values of 95% or higher up to a speed of 5000 r/min.

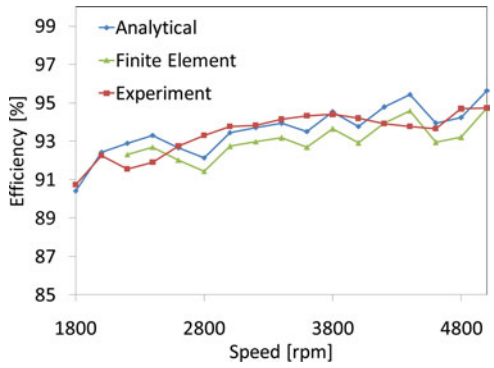

Fig. 21. Measured efficiency for FSCW-SPM machine under partial-load conditions.

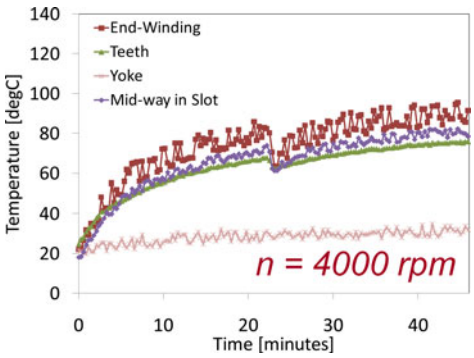

Fig. 22. Measured temperatures for the FSCW-SPM machine under rated-load conditions at 4000 r/min.

The efficiency of the FSCW-SPM under the partial-load condition (20% of rated torque) is similar to that of the FSCW-IPM machine (see Fig. 21). The efficiency is in the vicinity of 94% over the speed range up to 4800 r/min.

As with the FSCW-IPM machine, heat runs were carried out on the FSCW-SPM machine at 4000 r/min, as shown in Fig. 22. The machine temperature rise is in the vicinity of 60 °C without the presence of liquid cooling on the stator side. The end winding in the FSCW-SPM machine experiences the highest temperature due to the absence of direct cooling. This test shows that the motor could operate under steady-state conditions of 30 kW at 4000 r/min with only forced air cooling without exceeding temperature limits.

VI. Comparison of the Two Machines

As previously mentioned, it is quite possible that the mechanical losses are different for the two machines due to differences between the motor mechanical designs and also drivetrains of the two dynamometers. To eliminate this source of discrepancy, the two machines are compared in terms of their predicted electrical efficiencies. The predicted efficiencies of the two machines under rated-load conditions are shown in Fig. 23. The IPM machine is predicted to be more efficient by approximately 0.5% at lower speeds, while the SPM machine is more efficient at higher speeds, though only by 1%. Neither machine emerges as clearly superior in terms of efficiency since the impact of the mechanical losses would cause these predicted differences to be

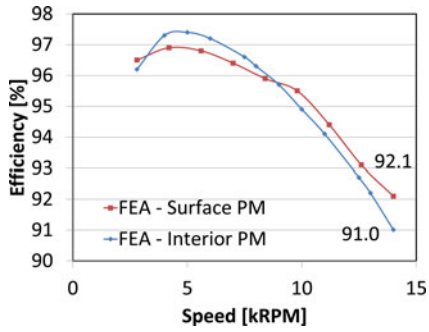

Fig. 23. Comparison of predicted electrical efficiencies of the two FSCW machines under rated-load condition.

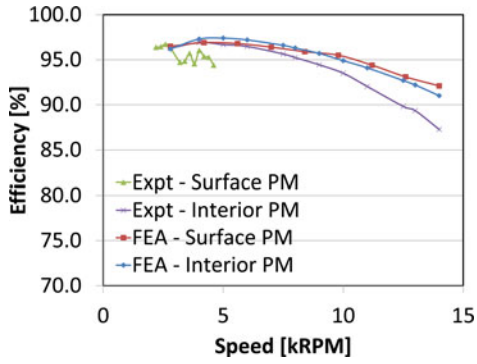

Fig. 24. Comparison of experimental electrical efficiencies of the two FSCW machines under rated-load conditions.

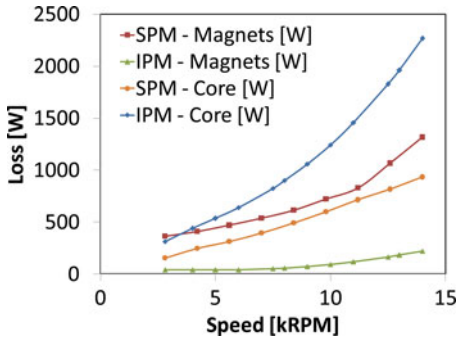

Fig. 25. Comparison of predicted core and magnet losses for the two FSCW machines under rated-load conditions.

marginal over the full speed range. However, it is noteworthy that the two motors achieve such similar efficiency values since the loss components are clearly different in the two motors.

In order to understand the effect of mechanical losses on the efficiency, the experimental efficiencies are overlaid in Fig. 24. The experimental efficiency with the SPM machine clearly falls lower than the prediction by at least a couple of percent of power. However, at this point, it is unclear if the additional losses are due to the electrical or mechanical causes. Further means of resolving this issue would be to use similar approach as the IPM machine i.e., using a dummy rotor for mechanical losses.

A clearer understanding is obtained comparing the predicted electrical losses under rated-load conditions, as shown in Fig. 25. As previously mentioned, the loss breakdown is different in the two machines. Due to the rich harmonic content of the

TABLE II
KEY MACHINES PARAMETERS AND DIMENSIONS

Parameter/Dimension	*FSCW-IPM*	*FSCW-SPM*	*Units*
Number of poles	10	10	
Number of slots	12	12	
Slots-per-pole-per-phase	2/5	2/5	
Stator outer diameter	237	274.2	mm
Rotor outer diameter	150	149.3	mm
Active Stack length	85	73.4	mm
Total length over end-turns	123	105	mm
Magnet height	7	11.5	mm
Airgap thickness (physical)	0.73	1	mm
Banding thickness	-	1.5	mm
Copper mass	7.5	7.5	Kg
Magnet mass	2.1	2.6	Kg
Total mass	27	27.8	Kg
Active material mass power density	2.03	2	kW/Kg
Characteristic current	130	125	Arms
Peak power output at 20% of maximum speed for 18 seconds and nominal voltage	55	55	kW
Continuous power output at 20 to 100% of maximum speed and nominal voltage	30	30	kW
Maximum per phase Current at motor	400	320	Arms
Back-emf at 100% of maximum speed, peak line-to-line voltage	800	673	Vpk

concentrated windings, the type of rotor matters little in terms of the overall losses. While the FSCW-SPM machine has higher losses in the magnets, the FSCW-IPM machine has higher losses in the stator and rotor cores. While the magnets in the IPM rotor are shielded by the iron, the reduced magnet losses are shifted into the iron. The corresponding results for partial-load conditions are similar to those for rated conditions and are not presented here.

Table II summarizes the key parameters, dimensions, and performance metrics of both machines. Since both machines are designed for the same set of specifications and for the same constant power speed range, they are very comparable in terms of mass, volume, and, hence, power density. This is consistent with some of the findings in [16]– [19]. Due to the reluctance torque component in the FSCW-IPM machine, it requires lower magnet mass. The FSCW-SPM machine exhibits better overload capability since it can produce the 55-kW peak power at 320 A_{rms} versus 400 A_{rms} in the FSCW-IPM machine. This is primarily attributed to lower magnetic saturation effects in the FSCW machine due to its larger effective air gap.

The flux density waveforms for each machine are shown in Figs. 26 and 27 for IPM machines, while the similar graphs for the SPM machine are shown in Figs. 28 and 29, respectively. The flux density waveform for the loaded condition of 100 A_{rms}, 50° gamma (for 2800 continuous power operating point) and the open-circuit waveform are shown in Fig. 26, while the flux density harmonic spectrum is shown in Fig. 27.

The similar waveforms for the SPM machine are shown in Figs. 28 and 29, respectively. The IPM machines show harmonic

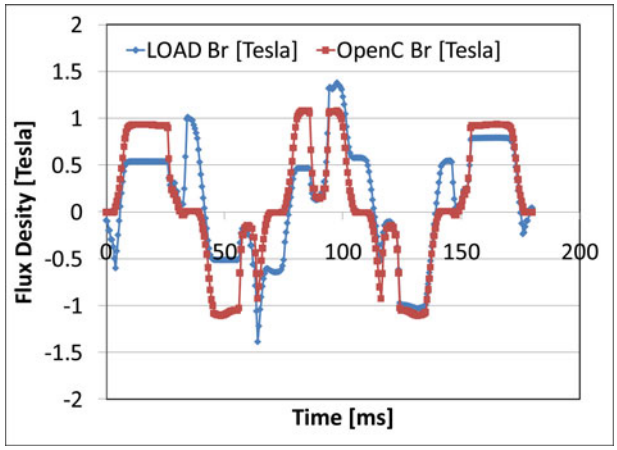

Fig. 26. Airgap flux density for FSCW-IPM machine at 2800 r/min.

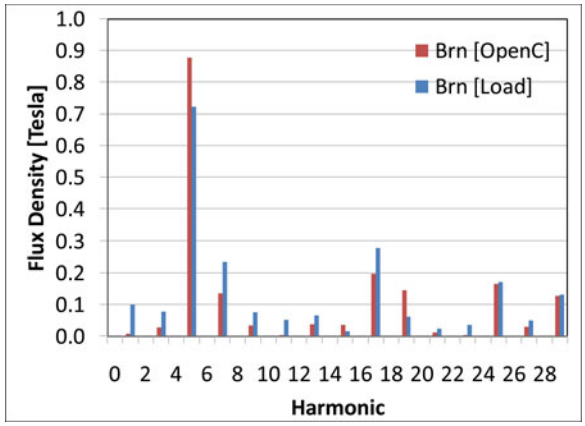

Fig. 27. Harmonic spectrum of Airgap flux density for FSCW-IPM machine at 2800 r/min.

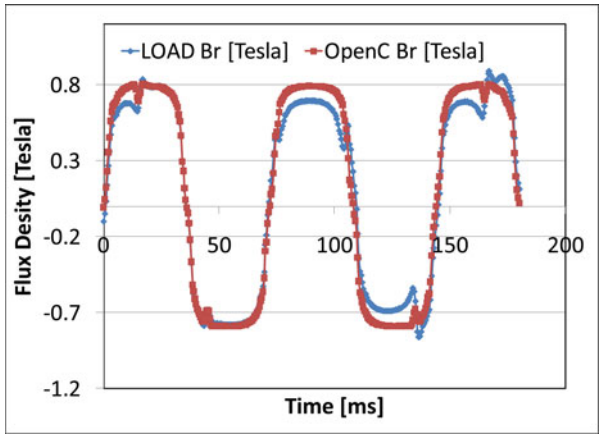

Fig. 28. Airgap flux density for FSCW-SPM machine at 2800 r/min.

numbers of 7th, 15th, 17th, and 19th, which are a source for additional iron losses in the IPM machine, while the SPM shown in Figs. 28 and 29, do not contain the 7th, 17th, and the 19th harmonic, respectively. These waveforms show that the iron losses in the rotor are more prominent in the IPM machine.

Figs. 30 and 31 show comparisons of the two FSCW machines to the FreedomCAR specifications and SoA machines (based on the test results published in [1]). Both FSCW machines have

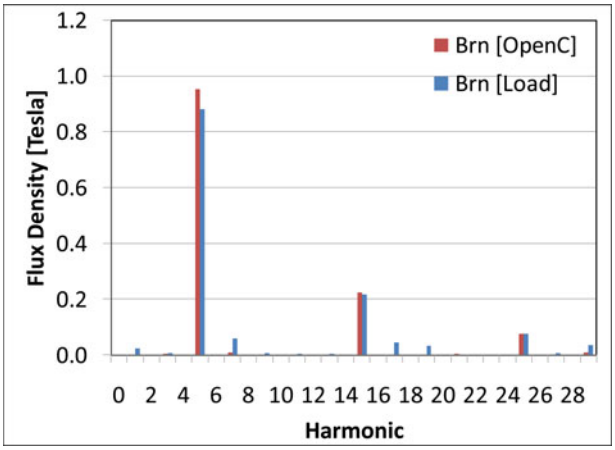

Fig. 29. Harmonic spectrum of Airgap flux density for FSCW-SPM machine at 2800 r/min.

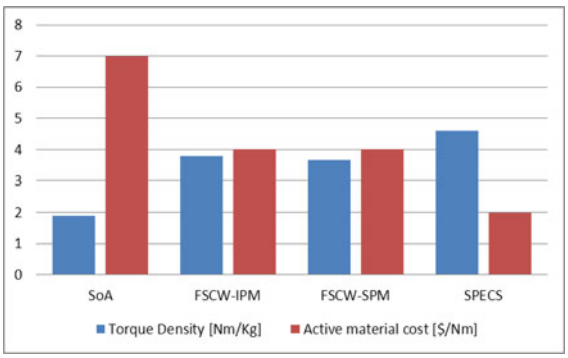

Fig. 30. Comparison of torque densities and active materials cost for the two FSCW machines with the state-of-the-art machines as well as the FreedomCar 2020 specifications.

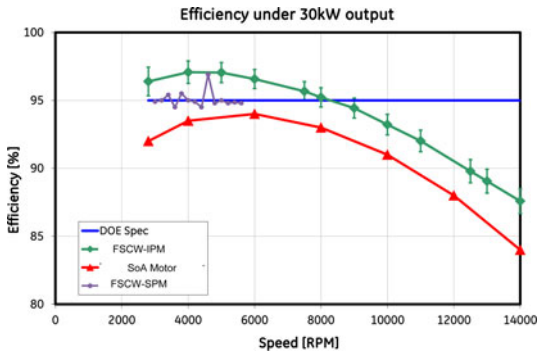

Fig. 31. Comparison of measured rated efficiencies for the two FSCW machines with the state-of-the-art machines as well as the FreedomCar 2020 specifications.

significantly higher continuous torque density (based on active mass) compared to the SoA machine, even though the FSCW machines have lower dc-bus voltage, 325 V, and higher coolant inlet temperatures, 105 °C, compared to the SoA machines that operate at 650-V dc-bus voltage and 65 °C coolant inlet temperatures.

Although the cost target is not currently met, the active material cost for the FSCW machines is significantly lower compared to the SoA machines. This is seen as a result of the thermal benefits arising from the lower copper losses in the FSCW machines, which also leads to size reduction.

Fig. 31 shows that both FSCW machines have comparable rated-load efficiency values. Even though the 95% efficiency target can be met only up to ∼9000 r/min, the efficiency at the maximum speed is significantly higher than the SoA machines.

VII. Conclusion

IPM and SPM machines equipped with FSCW can provide high performance and meet several of the very challenging FreedomCar 2020 specifications. Two machines, one interior PM and the other surface PM, were designed to meet these specifications. The analytical and experimental results for both machines have been compared and the design tradeoffs have been highlighted. The performance characteristics of both machines have also been compared to those of SoA traction motors. Based on the test results of the prototype machines built to date, the 30/55-kW 14 000-r/min advanced IPM- and SPM-FSCW machine architectures achieve significant improvements in full-load power density and efficiency compared to the SoA machines.

Acknowledgment

The authors would like to thank T. Bohn at Argonne National Laboratory for his support of the FSCW-SPM machine development.

References

[1] M. Olszewski, "Evaluation of the 2007 Toyota Camry hybrid synergy drive system," Oak Ridge Nat. Lab., Oak Ridge, TN, Tech. Rep. ORNL/TM-2007/190, 2008.

[2] J. Cros and P. Viarouge, "Synthesis of high performance PM motors with concentrated windings," *IEEE Trans. Energy Convers.*, vol. 17, no. 2, pp. 248–253, Jun. 2002.

[3] M. Kamiya, "Development of traction drive motors for the Toyota hybrid system," *IEEJ Trans. Ind. Appl.*, vol. 126, no. 4, pp. 473–479, 2006.

[4] A. M. EL-Refaie and T. M. Jahns, "Optimal flux weakening in surface PM machines using concentrated windings," *IEEE Trans. Ind. Appl.*, vol. 41, no. 3, pp. 790–800, May/Jun. 2005.

[5] A. M. EL-Refaie, T. M. Jahns, P. J. McCleer, and J. W. McKeever, "Experimental verification of optimal flux weakening in surface PM machines using concentrated windings," *IEEE Trans. Ind. Appl.*, vol. 42, no. 2, pp. 443–453, Mar./Apr. 2006.

[6] B. C. Mecrow, A. G. Jack, J. A. Haylock, and J. Coles, "Fault-tolerant permanent magnet machine drives," *IEE Proc.—Electr. Power Appl.*, vol. 143, no. 6, pp. 437–442, Nov. 1996.

[7] K. Atallah, D. Howe, P. H. Mellor, and D. A. Stone, "Rotor loss in permanent-magnet brushless AC machines," *IEEE Trans. Ind. Appl.*, vol. 36, no. 6, pp. 1612–1618, Nov./Dec. 2000.

[8] J. D. Ede, K. Atallah, G. W. Jewell, J. B. Wang, and D. Howe, "Effect of axial segmentation of permanent magnets on rotor loss of modular brushless machines," in *Proc. Conf. Rec. IEEE Ind. Appl. Soc. Annu. Meet.*, Oct. 2004, vol. 3, pp. 1703–1708.

[9] A. M. EL-Refaie, M. R. Shah, J. P. Alexander, S. Galioto, K.-K. Huh, and W. D. Gerstler, "Rotor end losses in multi-phase fractional-slot concentrated-winding permanent magnet synchronous machines," in *Proc. IEEE Energy Convers. Congr. Expo.*, Sep. 12–16, 2010, pp. 1312–1320.

[10] A. M. El-Refaie, M. R. Shah, R. Qu, and J. Kern, "Effect of number of phases on conducting sleeve losses of high-speed surface PM machine rotors," *IEEE Trans. Ind. Appl.*, vol. 44, no. 5, pp. 1522–1530, Sep./Oct. 2008.

[11] M. R. Shah and A. M. EL-Refaie, "Eddy current loss minimization in conducting sleeves of high speed machine rotors by optimal axial segmentation and copper cladding," in *Proc. Conf. Rec. IEEE Ind. Appl. Soc. Annu. Meet.*, New Orleans, LA, Sep. 2007, pp. 544–551.

[12] M. R. Shah and A. M. EL-Refaie, "End effects in multi-phase fractional-slot concentrated-winding surface permanent magnet synchronous

machines," in *Proc. Energy Convers. Congr. Expo.*, San Jose, CA, Sep. 2009, pp. 3798–3805.
[13] S. J. Park, H. W. Park, M. H. Lee, and F. Harashima, "A new approach for minimum-torque-ripple maximum-efficiency control of BLDC motor," *IEEE Trans. Ind. Electron.*, vol. 47, no. 1, pp. 109–114, Feb. 2000.
[14] C. W. Lu, B. J. Chalmers, A. C. Renfrew, and S. Huang, "Novel approach to current profiling for AC permanent magnet motors," *IEEE Trans. Energy Convers.*, vol. 14, no. 4, pp. 1294–1299, Dec. 1999.
[15] Z. Q. Zhu, D. Howe, and C. C. Chan, "Improved analytical model for predicting the magnetic field distribution in brushless PM machines," *IEEE Trans. Magn.*, vol. 38, no. 1, pp. 229–238, Jan. 2002.
[16] P. B. Reddy, T. M. Jahns, P. J. McCleer, and T. P. Bohn, "Design, analysis and fabrication of a high-performance fractional-slot concentrated winding surface PM machine," in *Proc. IEEE Energy. Conv. Congr. Expo.*, Atlanta, GA, Sep. 2010, pp. 1074–1081.
[17] W. L. Soong, P. B. Reddy, A. M. EL-Refaie, T. M. Jahns, and N. Ertugrul, "Surface PM machine parameter selection for wide field-weakening applications," in *Proc. Conf. Rec. IEEE Ind. Appl. Conf.*, Sep., 2007, pp. 882–889.
[18] W. Soong and T. J. E. Miller, "Field weakening performance of brushless synchronous AC motor drives," *Proc. IEE—Electr. Power Appl.*, vol. 141, no. 6, pp. 331–340, Nov. 1994.
[19] A. Vagati, G. Pellegrino, and P. Guglielmi, "Comparison between SPM and IPM motor drives for EV application," in *Proc. Int. Conf. Electr. Mach.*, Sep. 6–8, 2010, pp. 1–6.

Patel B. Reddy (S'07–M'10) received the Bachelor's degree in electrical engineering from the Indian Institute of Technology, Kharagpur, India, in 2003, during which he worked in the area of stability of power electronic converters. He received the Ph.D. degree in electrical and computer engineering from the University of Wisconsin-Madison, Madison, in 2010.

From 2004 to 2010, he was a Research Assistant with the Wisconsin Electric Machines and Power Consortium. Since 2010, he has been with the Electrical Machines Laboratory, General Electric Global Research Center, Niskayuna, NY. His interests include electrical machines and drives.

Ayman M. El-Refaie (S'95–M'05–SM'07) received the B.S and M.S degrees in electrical power engineering from Cairo University, Giza, Egypt, in 1995 and 1998, respectively, and the M.S. and Ph.D. degrees in electrical engineering from the University of Wisconsin-Madison, Madison, in 2002 and 2005, respectively.

Since 2005, he has been a Senior Engineer at the Electrical Machines and Drives Laboratory, General Electric Global Research Center, Niskayuna, NY. Between 1999 and 2005, he was a Research Assistant at the University of Wisconsin-Madison in the Wisconsin Electric Machines and Power Electronics Consortium group. Between 1995 and 1998, he was an Assistant Lecturer at Cairo University and the American University in Cairo. His interests include electrical machines and drives. He has 25 journal and 39 conference publications, with several others pending. He has 13 issued U.S. patents and 25 U.S. patent applications with several others pending. At General Electric, he has worked on several projects that involve the development of advanced electrical machines for various applications including, aerospace, traction, wind, and water desalination. He was the Program Manager and Principal Investigator of a $5.6 Million Department of Energy (DOE)-funded project to develop next generation traction motors for hybrid vehicles. He is currently the Program Manager and Principal Investigator of a $12 Million DOE-funded project to develop next-generation traction motors for hybrid vehicles that do not include rare-earth materials.

Dr. El-Refaie received several management awards at General Electric including the prestigious 2011 Albert W Hull Award, the highest individual award for early career researchers. He also received "The 2009 Forward Under 40" from the Wisconsin Alumni Association awarded to outstanding University of Wisconsin alumni under the age of 40 and the IEEE Industry Applications Society (IAS) "2009 Andrew Smith Outstanding Young Member Award." He is currently the Vice Chair for the IEEE IAS Transportation Systems Committee and an Associate Editor for the Electric Machines Committee. He was a Technical Program Chair for the IEEE 2011 Energy Conversion Conference and Exposition (ECCE). He will be the General Chair for ECCE 2014. He is a member of Sigma Xi.

Kum-Kang Huh (S'03–M'09) was born in Seoul, Korea. He received the B.S. and M.S. degrees in control and instrumentation engineering from Korea University, Seoul, in 1993 and 1995, respectively, and the Ph.D. degree in electrical engineering from the University of Wisconsin-Madison, Madison, in 2008.

Since 2008, he has been with the General Electric Global Research Center, Niskayuna, NY, where he is an Electrical Engineer with the Electric Power and Propulsion Systems Laboratory. Between 1995 and 2002, he was with the Mando R&D Center, Korea, where he developed electric vehicle traction systems and electric power steering systems. His research interests include modeling, controls, and diagnostics of electric machines, and power electronics systems.

Jagadeesh K. Tangudu (S'08–M'11) received the B.E. degree from Andhra University, Visakhapatnam, India, the M.E. degree from Indian Institute of Science Bangalore, Bangalore, India, and the M.S. and Ph.D. degrees in electrical and computer engineering from University of Wisconsin-Madison, Madison.

Since 2011, he has been with United Technologies research Center, East Hartford, CT, developing advanced electrical machines for various UTC businesses including wind, elevator, and air conditioners. Prior to his doctoral thesis work, he worked with GE Global Research Center and GE Energy for four years working on large turbo generator, next-generation locomotive motors. He has nine conference papers.

Thomas M. Jahns (S'73–M'79–SM'91–F'93) received the S.B. and S.M. degrees in 1974 and the Ph.D. degree in 1978 from the Massachusetts Institute of Technology, Cambridge, all in electrical engineering.

He joined the Faculty of the University of Wisconsin-Madison, Madison, in 1998 as a Professor in the Department of Electrical and Computer Engineering, where he is also an Associate Director of the Wisconsin Electric Machines and Power Electronics Consortium. Prior to coming to University of Wisconsin-Madison, he was with GE Corporate Research and Development (now GE Global Research Center) in Schenectady, NY, for 15 years, where he pursued new power electronics and motor drive technology in a variety of research and management positions. His research interests include permanent magnet synchronous machines for a variety of applications ranging from high-performance machine tools to low-cost appliance drives. During 1996–1998, he conducted a research sabbatical at the Massachusetts Institute of Technology, where he directed research activities in the area of advanced automotive electrical systems and accessories as a Co-Director of an industry-sponsored automotive consortium.

Dr. Jahns is the recipient of the 2005 IEEE Nikola Tesla Award. He received the William E. Newell Award by the IEEE Power Electronics Society (PELS) in 1999. He has been recognized as a Distinguished Lecturer by the IEEE Industry Applications Society during 1994–1995 and by IEEE-PELS during 1998–1999. He has served as the President of PELS (during 1995–1996) and Division II Director on the IEEE Board of Directors (during 2001–2002).